

PAPER • OPEN ACCESS

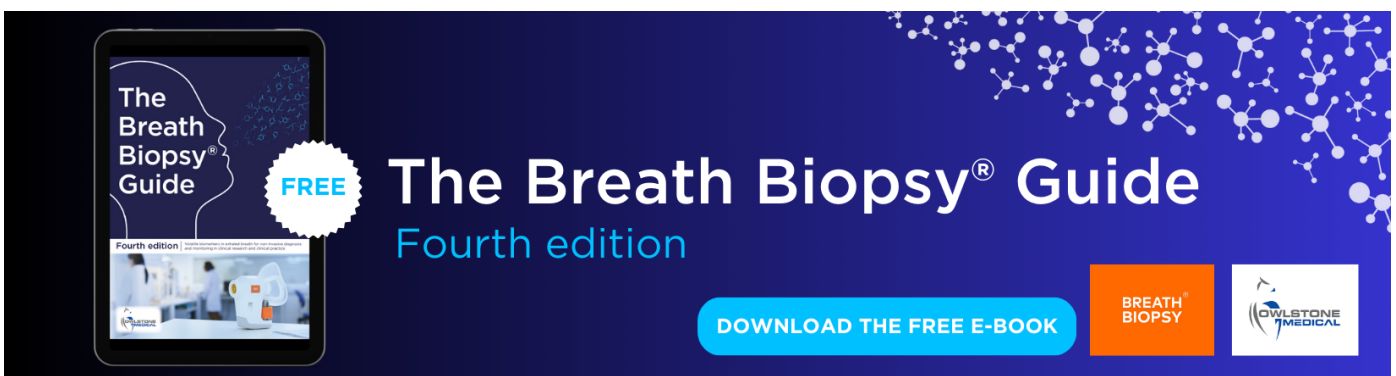
## Trilayer composite scaffold for urethral reconstruction: *in vitro* evaluation of mechanical, biological, and angiogenic properties

To cite this article: Tariq O Abbas *et al* 2024 *Biomed. Mater.* **19** 025022

View the [article online](#) for updates and enhancements.

### You may also like

- [Bi-layered calcium phosphate cement-based composite scaffold mimicking natural bone structure](#)  
Fupo He and Jiandong Ye
- [Egg white improves the biological properties of an alginate-methylcellulose bioink for 3D bioprinting of volumetric bone constructs](#)  
Suihong Liu, David Kilian, Tilman Ahlfeld *et al.*
- [Long-term biological performance of injectable and degradable calcium phosphate cement](#)  
Eline-Claire Grosfeld, Jan Willem M Hoekstra, Ralf-Peter Herber *et al.*



The Breath Biopsy® Guide  
Fourth edition

FREE

DOWNLOAD THE FREE E-BOOK

BREATH BIOPSY

OWLSTONE MEDICAL

# Biomedical Materials



## PAPER

### OPEN ACCESS

RECEIVED  
8 August 2023

REVISED  
22 November 2023

ACCEPTED FOR PUBLICATION  
9 January 2024

PUBLISHED  
25 January 2024

Original content from this work may be used under the terms of the [Creative Commons Attribution 4.0 licence](https://creativecommons.org/licenses/by/4.0/).

Any further distribution of this work must maintain attribution to the author(s) and the title of the work, journal citation and DOI.



## Trilayer composite scaffold for urethral reconstruction: *in vitro* evaluation of mechanical, biological, and angiogenic properties

Tariq O Abbas<sup>1,2,3,4,5</sup> , Hemalatha Parangusan<sup>6</sup>, Huseyin C Yalcin<sup>7,8</sup> , Mohamed Hassan<sup>6</sup> , Lubna Zakrif<sup>7</sup>, Nooshin Zandi<sup>1</sup> and Cristian P Pennisi<sup>1,\*</sup>

<sup>1</sup> Regenerative Medicine Group, Department of Health Science and Technology, Aalborg University, Aalborg, Denmark

<sup>2</sup> Pediatric Surgery Department, Hamad General Hospital, Doha, Qatar

<sup>3</sup> College of Medicine, Qatar University, Doha, Qatar

<sup>4</sup> Weill Cornell Medicine-Qatar, Doha, Qatar

<sup>5</sup> Urology Division, Urology Department, Sidra Medicine, Doha, Qatar

<sup>6</sup> Centre for Advanced Materials, Qatar University, Doha, Qatar

<sup>7</sup> Biomedical Research Centre, Qatar University, Doha, Qatar

<sup>8</sup> Department of Biomedical Science, College of Health Sciences, QU Health, Qatar University, Doha, Qatar

\* Author to whom any correspondence should be addressed.

E-mail: [cpennisi@hst.aau.dk](mailto:cpennisi@hst.aau.dk)

**Keywords:** tissue engineering, urethral reconstruction, hybrid scaffolds, chitosan, angiogenesis

### Abstract

Regeneration of damaged urethral tissue remains a major challenge in the field of lower urinary tract reconstruction. To address this issue, various synthetic and natural biodegradable biomaterials are currently being explored for the fabrication of scaffolds that promote urethral regeneration and healing. In this study, we present an approach to fabricate a trilayer hybrid scaffold comprising a central layer of poly(lactic acid) (PLA) between two layers of chitosan. The chitosan/PLA/chitosan (CPC) scaffolds were fabricated by a sequential electrospinning process and their properties were evaluated for their suitability for urethral tissue engineering. The physical and biological properties of the CPC scaffolds were evaluated in comparison to electrospun PLA scaffolds and acellular dermis (Alloderm) as controls for a synthetic and a natural scaffold, respectively. Compared to the controls, the CPC scaffolds exhibited higher elastic modulus and ultimate tensile strength, while maintaining extensibility and suture retention strength appropriate for clinical use. The CPC scaffolds displayed significant hydrophilicity, which was associated with a higher water absorption capacity of the chitosan nanofibres. The degradation products of the CPC scaffolds did not exhibit cytotoxicity and promoted wound closure by fibroblasts *in vitro*. In addition, CPC scaffolds showed increased growth of smooth muscle cells, an essential component for functional regeneration of urethral tissue. Furthermore, in a chicken embryo-based assay, CPC scaffolds demonstrated significantly higher angiogenic potential, indicating their ability to promote vascularisation, a crucial aspect for successful urethral reconstruction. Overall, these results suggest that CPC hybrid scaffolds containing both natural and synthetic components offer significant advantages over conventional acellular or synthetic materials alone. CPC scaffolds show promise as potential candidates for further research into the reconstruction of the urethra *in vivo*.

### 1. Introduction

Anomalies of the urethra may be either congenital or acquired later in life and present a major challenge to urologists. For example, hypospadias is a common defect of the external genitalia that occurs in approximately 1 in 200 live male births and results in significant narrowing of the urethra that often requires

surgical correction [1, 2]. Urethroplasty with a buccal mucosal graft may be effective in severe cases or for patients who experience postoperative complications, but there are no generally accepted algorithms yet for the surgical management of hypospadias [1, 3–5]. Tissue engineering offers promising solutions to produce grafts that closely resemble the natural architecture of the urethra [6, 7].

The normal human urethra has a tubular structure consisting of three distinct layers: (i) epithelium (innermost layer), which consists of transitional cells that act as a barrier to urine, (ii) submucosa (middle layer), which consists mainly of fibroblasts that provide structural strength to the urethral wall, and (iii) muscle layer (outermost layer), which contains smooth muscle cells (SMCs) that provide contractility to maintain the high compliance of the urethra during urination [8, 9]. Most tissue engineering studies to date have constructed cell-seeded or acellular scaffolds that aim to reconstruct the epithelial and muscle layers, often ignoring the submucosa and the critical role of the surrounding corpus spongiosum in providing mechanical support and blood supply [10–13]. The corpus spongiosum is inadequate in hypospadias [14, 15], so failure to replace this tissue may lead to long-term failure of urethral reconstruction [16]. Therefore, it is essential to develop tissue engineering strategies that involve all layers of the urethra. By combining these essential components, more effective surgical repair can be achieved, leading to better functional outcomes in urethral tissue regeneration.

In recent decades, various natural and synthetic biodegradable scaffolds have been investigated for urethral tissue engineering, including scaffolds seeded with primary cells [17–20]. Synthetic polymers exhibit high strength but are less biocompatible, whereas natural biomaterials exhibit the opposite properties [21]. Synthetic polyesters such as poly(lactic acid) (PLA) have been widely used for scaffold fabrication because they can be easily degraded to lactic acid by simple hydrolysis [22]. In addition, PLA scaffolds can successfully support cell growth in regenerative medicine applications [23, 24]. Although PLA is typically hydrophobic [25], the polymer exhibits excellent mechanical strength that can be tailored to a range of clinical applications and has been approved by the Food and Drug Administration. However, a major limitation of PLA and its co-polymers is their insufficient biocompatibility in urethral replacement, which often leads to undesirable inflammatory reactions when used *in vivo* [26].

Recent advances in tissue engineering have shown that it is possible to develop more physiological grafts, such as synthetic scaffolds of microfibrillar PLA and nanofibrillar poly(3-hydroxybutyrate-co-3-hydroxyvalerate), which have been proposed for the fabrication of tissue substitutes for buccal mucosa exhibiting good mechanical properties and morphological similarity to normal human oral mucosa [27]. Another promising strategy to improve the biological performance of synthetic polymers has been to combine them with natural polymers [28]. Commonly used natural polymers are cellulose,

chitin, silk fibroin, and gelatin. Chitin is the second most abundant biopolymer after cellulose [29] and is commonly found in invertebrates, green algae, and fungi [30]. Deacetylation of chitin produces the polysaccharide chitosan, which can be used to produce multilayer films by a layer-by-layer deposition technique [31]. Chitosan is degraded *in vivo* by lysozyme and various other enzymes [32], resulting in the formation of nontoxic oligosaccharides of varying lengths that can be incorporated (or simply excreted) into normal tissue metabolic pathways [33]. Chitosan also exhibits significant antimicrobial activity [34] and thus may be particularly well suited as a biomaterial for urologic applications, which to our knowledge has not yet been investigated. Although it is difficult to produce chitosan alone as electrospun nanofibers, this material can be blended with other polymers such as poly(ethylene oxide) (PEO) or poly(vinyl alcohol) to improve fiber stability [35]. PEO is a synthetic biopolymer approved for use in food, cosmetics, personal care products, and pharmaceuticals. The addition of PEO reduces the viscosity of the chitosan solution, allowing it to be electrospun at high polymer concentrations. Hybrid scaffolds combining synthetic with natural biomaterials can therefore help to overcome important technical problems and offer numerous material advantages in the clinic [36].

Insufficient angiogenesis and poor epithelialization are the major challenges in urethral regeneration with conventional tissue-engineered grafts. An ideal tissue engineered urethra should promote sufficient angiogenesis to support epithelialization and regeneration of the urethra *in vivo*. At the site of the primary defect, urothelial cells must migrate and cover the affected area to form new epithelium, which requires parallel vascularization to provide sufficient nutrients and oxygen. The formation of epithelium is critical to the structure and function of the urethra because it provides an essential barrier to the cytotoxic components of urine that can cause fibrosis, shrinkage, and eventually stricture [37]. Consequently, a priority in the development of scaffold materials is to synthesize multilayer grafts that can support multiple healing processes in parallel. We hypothesized that PLA/chitosan composite scaffolds could represent a novel ‘off-the-shelf’ scaffold with structural and mechanical properties that initially stabilize tissue function and, over time, would allow gradual regeneration of the damaged urethra. The aim of our study was to investigate the potential of chitosan/PLA/chitosan (CPC) hybrid scaffolds for improved urethral tissue regeneration, focusing on the *in vitro* evaluation of their physical and biological properties and comparing them with conventional acellular and synthetic materials.

## 2. Materials and methods

### 2.1. Chemicals and materials

Chemicals purchased from Sigma Aldrich included chitosan (deacetylated chitin, poly(D-glucosamine), 75%–85% degree of deacetylation), PEO (MW = 600 000–1000 000), glacial acetic acid, cetrimonium bromide (CTAB), dichloromethane (DCM), and dimethylformamide (DMF). The PLA (Ingeo Biopolymer 2003D) was purchased from NatureWorks (Minnetonka, MN, USA). Acellular dermal matrix scaffolds (AlloDerm<sup>®</sup>, designated ALD) were obtained from LifeCell Corp (Branchburd, NJ, USA).

### 2.2. Preparation of electrospun scaffolds

A PLA solution (10% w/v) was prepared by adding PLA pellets to a 70:30 mixture of DCM and DMF with stirring for 6 h at room temperature. A chitosan solution (2% w/v) was prepared by dissolving chitosan in a mixture of acetic acid, DCM, and distilled water (4:5:1) and a PEO solution was prepared by dissolving PEO (2% w/v) in a mixture of acetic acid and distilled water (1:1). The polymer solutions were prepared separately under continuous magnetic stirring for 6 h at room temperature to obtain homogeneous solutions. To determine the optimal mixture for the preparation of small diameter fibers without beads, the chitosan and PEO solutions were combined in different ratios (60:40, 50:50, 70:30, or 80:20) with additional magnetic stirring for 4 h. CTAB was dissolved in the chitosan:PEO mixture at a final concentration of 40 mM.

Scaffolds were manufactured using a nanofiber electrospinning machine (Tong Li Tech, Shenzhen, China). The PLA scaffolds were fabricated at a flow rate of 2 ml h<sup>-1</sup>, a distance of 12 cm between the needle tip and the collector, and an applied voltage of 12 kV. To fabricate the trilayer CPC scaffold, the first layer solution consisting of chitosan:PEO was filled into a 10 ml syringe and electrospun at a flow rate of 0.3 ml h<sup>-1</sup>. The nanofibers were collected on an aluminium substrate at a distance of 10 cm between the needle tip and the collector at an applied voltage of 18 kV. Then, the second layer of PLA solution was filled into a 20 ml syringe and electrospun directly on the first layer at a flow rate of 2 ml h<sup>-1</sup>, a distance of 12 cm between the needle tip and the collector, and an applied voltage of 12 kV. Finally, the third layer consisting of chitosan:PEO was immediately electrospun to overlay the previous layers. To improve the stability of the chitosan nanofibers, the CPC scaffolds were immersed in 90:10 methanol/water for 20 min before allowing this to dry at room temperature inside a fume hood [38]. A schematic diagram of the sequential fabrication process of the CPC scaffolds is depicted in figure 1(a).

### 2.3. Morphological analysis of the scaffolds

The morphology of the different nanofiber scaffolds was studied using a scanning electron microscope (SEM, XL-30E, Philips, The Netherlands). Samples with a size of (4 × 4) mm were sputtered with gold to increase conductivity and prevent the sample from being charged by the accumulation of static electric fields [39]. To visualize the cross-sectional morphology of the CPC scaffolds, they were broken after soaking in liquid nitrogen for 15 min. Fiber diameters were quantified using the ImageJ plugin DiameterJ [40] based on four independent SEM images per scaffold type.

### 2.4. Mechanical testing of the scaffolds

For the mechanical tests, all scaffolds were prepared as strips of (35 × 7) mm. A total of six strips of each scaffold type were tested. Mechanical testing was carried out in accordance with ISO: 604–02 using the universal testing machine (LF PLUS, LLOYD, UK) at an elongation rate of 5 mm min<sup>-1</sup> and load range of 5000 N. Prior to testing, all scaffolds were soaked in a phosphate-buffered saline (PBS) solution for 30 min. The Nexygen Plus software in the testing device was utilized to determine the Young's modulus by analyzing the slope of the first linear segment of the stress–strain curve. Additionally, the software was used to calculate the yield stress and extensibility.

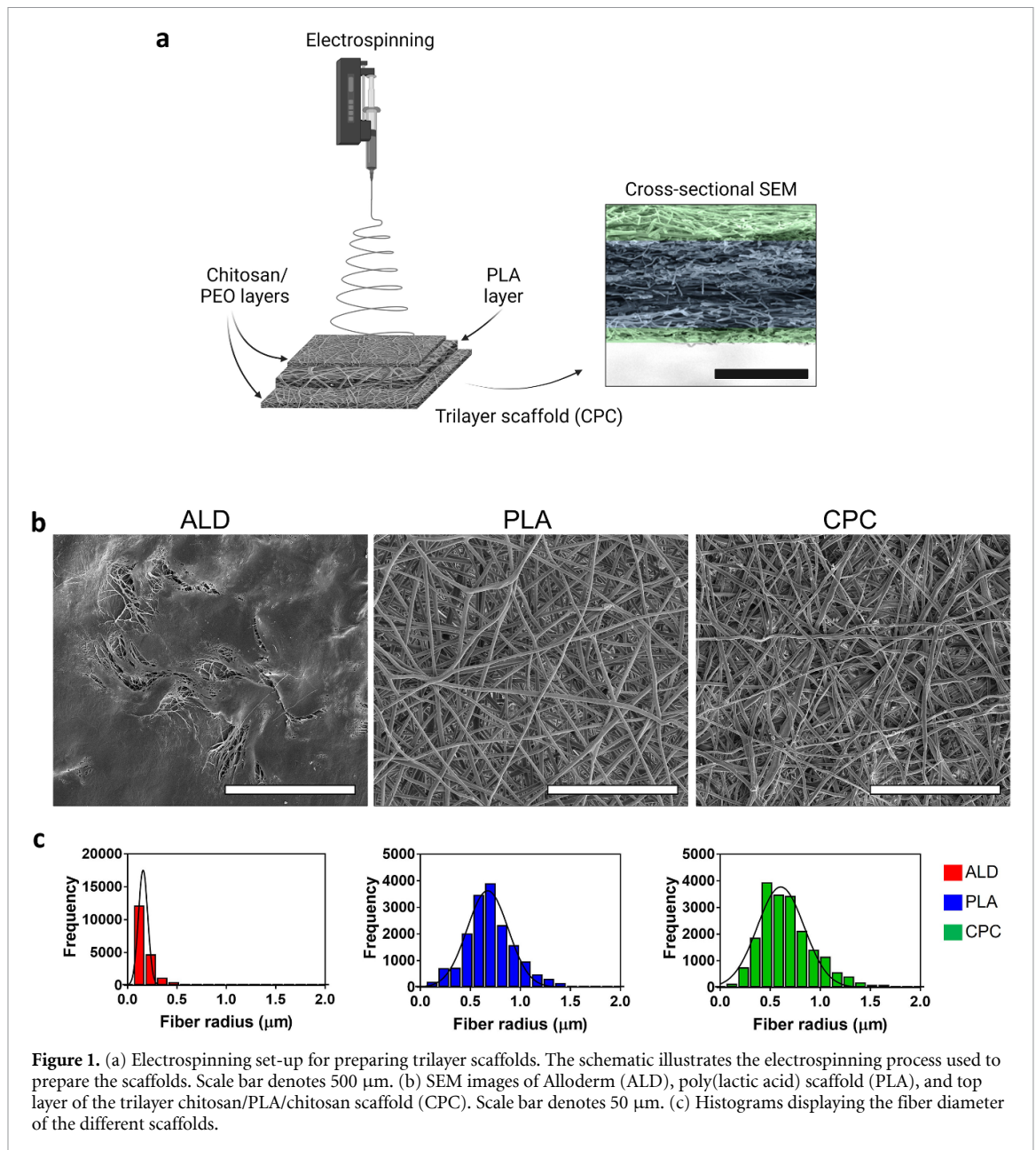
### 2.5. Suture retention test

The suture retention strength of each scaffold was quantified according to the VP20 standards of the American National Standard Institute-Association for the Advancement of Medical Instruments. Suture retention was assessed using the LF PLUS uniaxial force device using (35 × 10) mm test samples. One end of the sample was fixed to the lower grip of the device. A single 5–0 polydioxanone suture (Round Body, RB#2) was passed through the other end of the sample (3 mm below the cut edge). The two free ends of the suture were attached to the upper grip and pulled at a constant rate of 1 mm min<sup>-1</sup>. The suture-retention strength was defined as the peak force achieved during this procedure.

### 2.6. Scaffold swelling and *in vitro* degradation

The dry weight of the different scaffolds was measured with an electronic balance before they were transferred to separate closed containers with PBS. After specified time intervals (1, 2, 3, 4, 24, 48, 72, and 96 h), the samples were removed from the PBS and excess surface water was dried with tissue paper before being reweighed to determine the wet weight. Swelling was then calculated as a percentage of water uptake:

$$\text{Water uptake } [\%] = \left( \frac{W_s - W_d}{W_d} \right) \times 100$$



where  $W_s$  is sample wet weight, and  $W_d$  is dry weight of the same sample. At least three specimens were tested for each sample to obtain average values.

For the *in vitro* degradation tests, scaffolds were cut into (15  $\times$  15) mm samples. Four samples of each scaffold type were immersed in PBS and incubated at 37  $^{\circ}\text{C}$ . Samples were removed from PBS at various intervals (1–24 d), carefully washed with distilled water, and then dried at room temperature. Material dissolution was evaluated by weight loss and morphological changes relative to immersion time. Weight loss was determined by dividing the dry weight of the samples at a given time by the initial weight of the samples using the following equation:

$$\text{Weight loss (\%)} = \left( \frac{W_f}{W_i} \times 100 \right)$$

where  $W_i$  is the initial dry weight of the scaffold before immersion in PBS, and  $W_f$  is the final dry weight of the same specimen after being previously immersed in PBS for a variable duration.

### 2.7. Contact angle measurement

The hydrophilicity of the scaffolds was assessed by using a contact angle instrument device (OCA 35-Dataphysics). Deionized water droplets of 0.5  $\mu\text{l}$  were deposited onto each scaffold, and contact angles were measured four times from different positions to obtain an average value.

### 2.8. Cell sources and culture conditions

Cytocompatibility experiments were performed with NIH/3T3 fibroblasts obtained from the American Type Culture Collection, USA. Cells were cultured

in Dulbecco's Modified Eagle's Medium supplemented with 10% foetal bovine serum (FBS) and 0.1% penicillin/streptomycin. All experiments were performed with cells of passages 15–20. Cell growth experiments on the scaffolds were performed with SMCs from human bladder purchased from ScienCell Research Laboratories (Carlsbad, CA, USA). Cells were cultured in growth medium (GM) containing smooth muscle cell basal medium (ScienCell Research Laboratories) supplemented with 1% smooth muscle cell growth supplement, ScienCell Research Laboratories, 2% FBS, and 1% penicillin/streptomycin. Cell culture was performed in a humidified incubator (Thermo Fisher Scientific, USA) at 5% CO<sub>2</sub> and 37 °C. For all cell culture experiments, the test scaffolds were sterilized with UV irradiation for 20 min before addition to the culture wells.

### 2.9. Cytocompatibility assays

For the cytotoxicity assay, fibroblasts were seeded at a density of  $5 \times 10^3$  cells cm<sup>2</sup> in 6-well plates and cultured until confluency. Scaffolds were cut into (10 × 10) mm samples, placed in the wells, and incubated for 24 h. A live/dead cell viability and cytotoxicity kit (Molecular Probes, USA) was used to assess the effects of components released from the scaffolds on fibroblast viability. Live/dead stain was prepared by adding 1 μM ethidium homodimer-1 and 2 μM calcein-AM to serum-free medium. After discarding the supernatants and the scaffolds, cells were rinsed in PBS twice and treated with the live/dead stains for 1 h. The stained cells were observed under an inverted fluorescence microscope at 40× magnification (OLYMPUS IX –71, UK), and images were acquired using imaging software ZEN and an AxioCam camera (Carl Zeiss, Germany). Cell viability was calculated using the following equation:

$$\text{Viability (\%)} = \left( \frac{L}{L + D} \right) \times 100$$

where  $L$  and  $D$  represent the total number of live and dead cells per field, respectively. Experiments were performed in triplicate for each scaffold type.

To evaluate the effects of degradation components on fibroblast migration, a time-dependent analysis was performed. Fibroblasts were seeded in 12-well plates at a density of  $5 \times 10^5$  cells/well. When fibroblasts reached confluence, a scratch was made in the chambers using a 100 μl pipette tip. The chambers were then rinsed with PBS to remove all free-floating cells and debris. Scaffold samples of (10 × 10) mm were added to each well along with serum-free medium, and the plates were incubated for various time intervals. Images of the scratched areas were taken before scaffolds were placed and after 3, 6, and 24 h using an inverted microscope (Olympus

IX –71, UK). Experiments were performed in triplicate for each scaffold. Relative wound closure was calculated using the following formula:

$$\text{Relative wound closure (\%)} = 100 - \left[ \left( \frac{A_i - A_f}{A_f} \right) \times 100 \right]$$

where  $A_i$  and  $A_f$  define the area between scratch edges before and after time of incubation with each scaffold, respectively.

### 2.10. Assessment of growth of SMCs on the scaffolds

Scaffold samples of (10 × 10) mm were placed on 12-well plates and soaked in GM at 37 °C for 1 h. SMCs were trypsinized and 130 μl of cell suspension containing  $2 \times 10^5$  cells was added to the center of each scaffold. After incubation at 37 °C for 30 min, the scaffolds were flipped, and the seeding operation was repeated on the other side of the scaffolds. Subsequently, the culture wells were filled with GM and the plates were placed back in the incubator. The medium was replaced every other day. Five replicates of each scaffold type were used for testing. Cell viability was determined on days 1, 3, and 7 after seeding using a 3-(4,5-dimethylthiazol-2-yl)-2,5-diphenyltetrazolium bromide (MTT) assay (Sigma Aldrich, USA). Scaffolds were rinsed twice in PBS before a 5 mg ml<sup>-1</sup> solution of MTT in PBS was added to each well and incubated for 4 h. The reaction was stopped by discarding the reaction solution and dissolving the converted dye in dimethyl sulfoxide for 15 min. A total volume of 100 μl of purple solution was taken from each sample and transferred to a 96-well plate. Optical density (OD) was then measured at a wavelength of 570 nm using an EPOCH2 microplate reader (BioTek) according to the manufacturer's instructions. To quantify cell proliferation, the normalized OD was calculated by dividing the measured OD by the control OD. The average OD of the ALD scaffold at day 1 was used as a control. All experiments were repeated three times, and the OD values were measured in triplicate.

After 7 d of culture, the scaffolds were fixed in formalin 10% for histological analysis. Scaffolds were embedded in optimal cutting temperature (OCT) compound and frozen in liquid nitrogen. Cross sections (5 μm thickness) were cut using a cryostat (Leica CM300) and placed on frosted glass slides. The slides were then soaked in deionized water to remove the OCT, stained with haematoxylin, washed with running tap water, and stained with eosin. After another wash with tap water, samples were dehydrated in 70% alcohol and then placed in 100% alcohol. Finally, the slides were cleaned twice in xylene and mounted on a coverslip with DPX mounting medium. The sections were observed with a light microscope (Olympus IX –71, UK).

### 2.11. Assessment of the angiogenic capacity of the scaffolds

The chorioallantoic membrane (CAM) assay is a useful biological model for assessing angiogenic capacity of materials and compounds. Chick embryo experiments were conducted at Qatar University Biomedical Research Center under Qatar University IACUC Approval QU-IACUC 005/2021. Fertilized chicken (*Gallus gallus domesticus*) eggs were purchased from Arab Qatari Poltry Farm (Al-Khor, Qatar), stored at 12 °C–18 °C to prevent chick development during transport, and gradually brought to room temperature to prevent condensation in the egg. Eggs were incubated until day four at 37 °C from the day of fertilization in a 60% humidified egg incubator (1502-Digital Sportsman, GQF Manufacturing Company Inc.) with adjustable horizontal rotation (1 h schedule). Eggs were collected and cleaned at the planned surgical site with 70% ethanol. The amnion (4–5 ml) was aspirated through a small puncture with a needle, taking care not to injure the embryo, which was located by candling. Curved scissors were used to create a (15 × 20) mm window on the eggshell to allow access to the CAM. Sterile (10 × 10) mm samples of each scaffold type were placed on the exposed CAM surface ( $n = 6$ ). The exposed window was then covered with transparent adhesive tape and the egg was placed back into a 40% humidified portable incubator at 37 °C (Hovabator, GQF Manufacturing Company Inc.). After 24 h, vessel development was observed using a stereomicroscope (Stemi 508), and the number of branch points and vessel diameters were quantified using Angioquant software. Images were acquired at 10× magnification.

### 2.12. Statistical analysis

Results are presented as means ± standard deviation. Data were analyzed in IBM SPSS 23 software using independent-samples T tests and analysis of variance to identify differences between groups. Differences in mechanical properties were assessed with Friedman tests in GraphPad Prism 8 with Dunn test for multiple comparisons between groups.  $P$  values < 0.05 were considered statistically significant.

## 3. Results

### 3.1. Morphological characterization of the scaffolds

An initial evaluation of chitosan scaffolds by SEM revealed that not all formulations tested yielded suitable nanofibers (data not shown). Optimal fiber formation was achieved with a chitosan:PEO ratio of 60:40, which was used to prepare the CPC scaffolds in the remainder of this work. The cross-sectional SEM of the CPC scaffolds confirmed a cohesive tri-layer nanofibrous structure (figure 1(a)). The average thickness of the CPC scaffolds was  $1.10 \pm 0.19$  mm.

On the other hand, the PLA scaffolds had an average thickness of  $0.60 \pm 0.12$  mm, while the ALD scaffolds had a thickness of  $2.30 \pm 0.29$  mm. Figure 1(b) shows the SEM images of the different scaffold types. The electrospun CPC scaffolds show smooth nanofibers comparable in diameter and size distribution to the PLA scaffolds. Quantitative analysis revealed a normal distribution of fiber diameter. In contrast, the ALD samples showed a much more compact structure, with a narrow fiber size distribution (figure 1(c)).

### 3.2. Assessment of mechanical properties

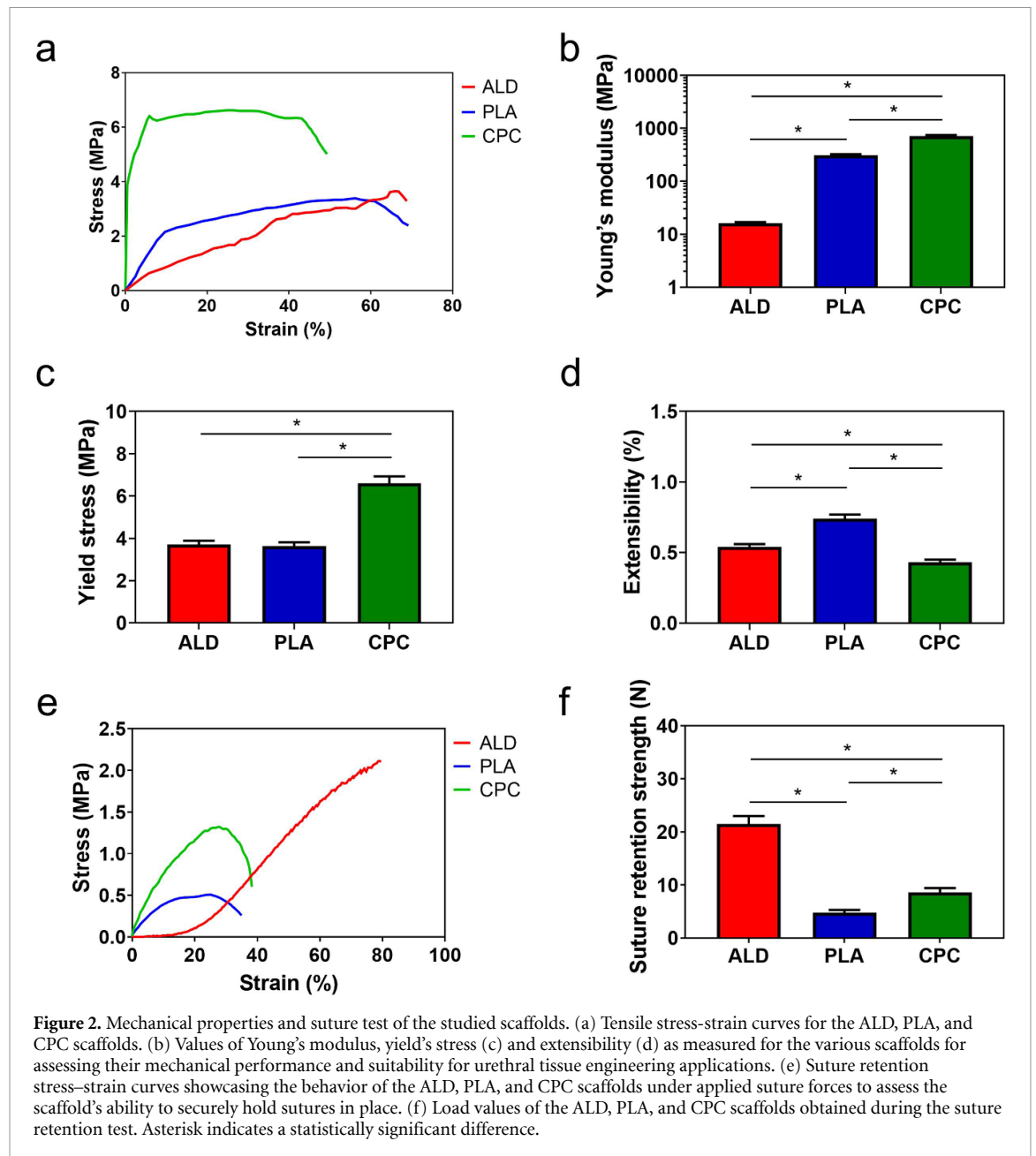
The stress–strain curve in figure 2(a) illustrates the relationship between the magnitude of applied stress and the resulting strain of the scaffold. CPC scaffolds showed a linear stress–strain characteristic until failure at high load. In contrast, the PLA scaffolds exhibited a less stiff behavior, while the ALD scaffolds exhibited the largest deformation at low stress. As shown in figure 2(b), the CPC scaffolds exhibited the highest Young's modulus as compared to the other two scaffold types. In addition, the CPC scaffolds exhibited the highest tensile strength while showing relatively low ductility with a strain tolerance of 44% before failure (figures 2(c) and (d)). The PLA scaffold, on the other hand, exhibited higher ductility with a strain tolerance of 62%, which can be attributed to the high plastic content of the scaffold. (figure 2(c)). To assess the ability of a scaffold to accept and retain suture material, the suture retention capacity was evaluated. CPC scaffolds exhibited higher retention than PLA, but lower retention than ALD scaffolds (figures 2(e) and (f)).

### 3.3. Scaffold wettability

The wettability of the scaffold surface has a major impact on the attachment, proliferation, and viability of many different adherent cell types. As shown in figure 3(b), contact angle measurements indicated that CPC was significantly more hydrophilic compared to the other scaffold types. There were no significant differences when comparing the wettability of the upper and lower chitosan layers comprising the CPC scaffolds.

### 3.4. Swelling and degradation

Scaffolds are exposed to aqueous solutions *in vivo*, which can cause swelling of the primary structure and alter their dimensions and mechanical properties. Figure 3(a) shows the morphological characteristics of the scaffolds before and after immersion in PBS for 48 h. Qualitative inspection of the SEM images revealed that the overall fiber morphology was not significantly altered. When assessing the swelling behavior, most of the swelling of the electrospun scaffolds occurred within 48 h of immersion and did not increase significantly with further immersion time. The CPC had a greater capacity to adsorb water than



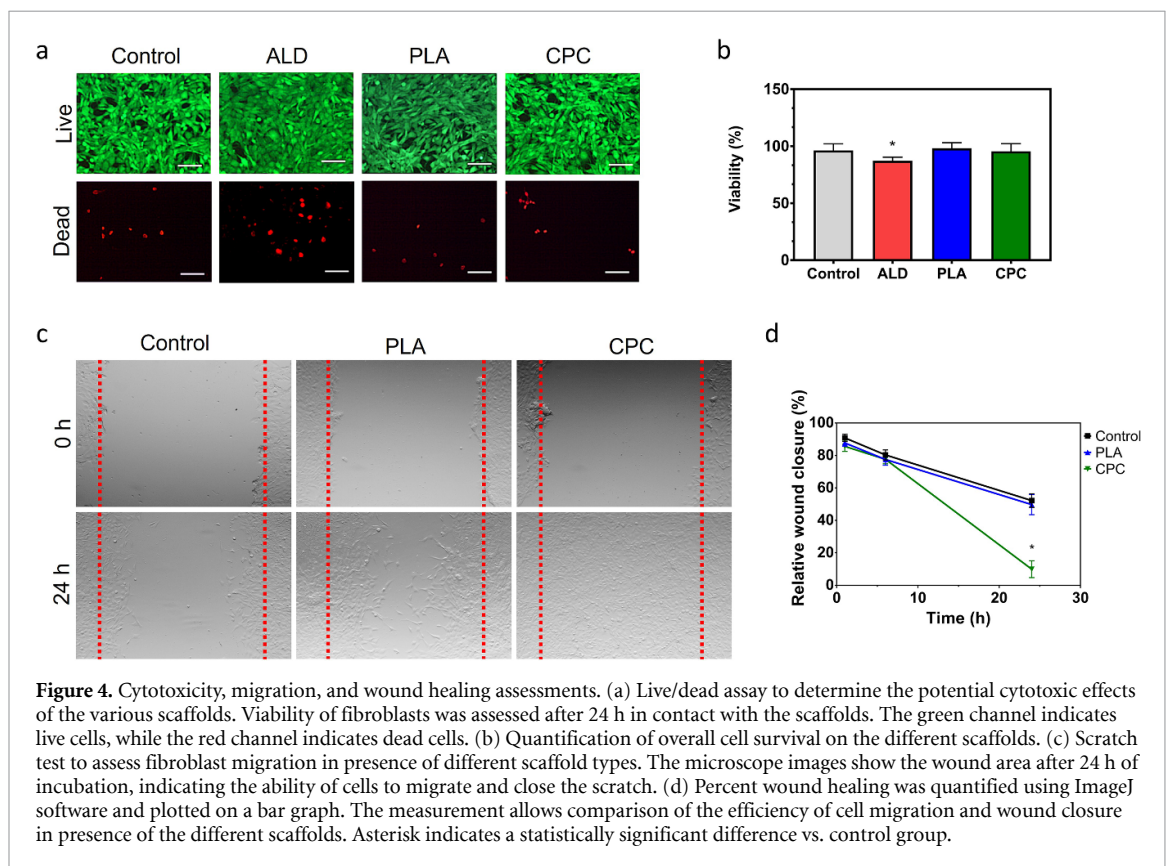
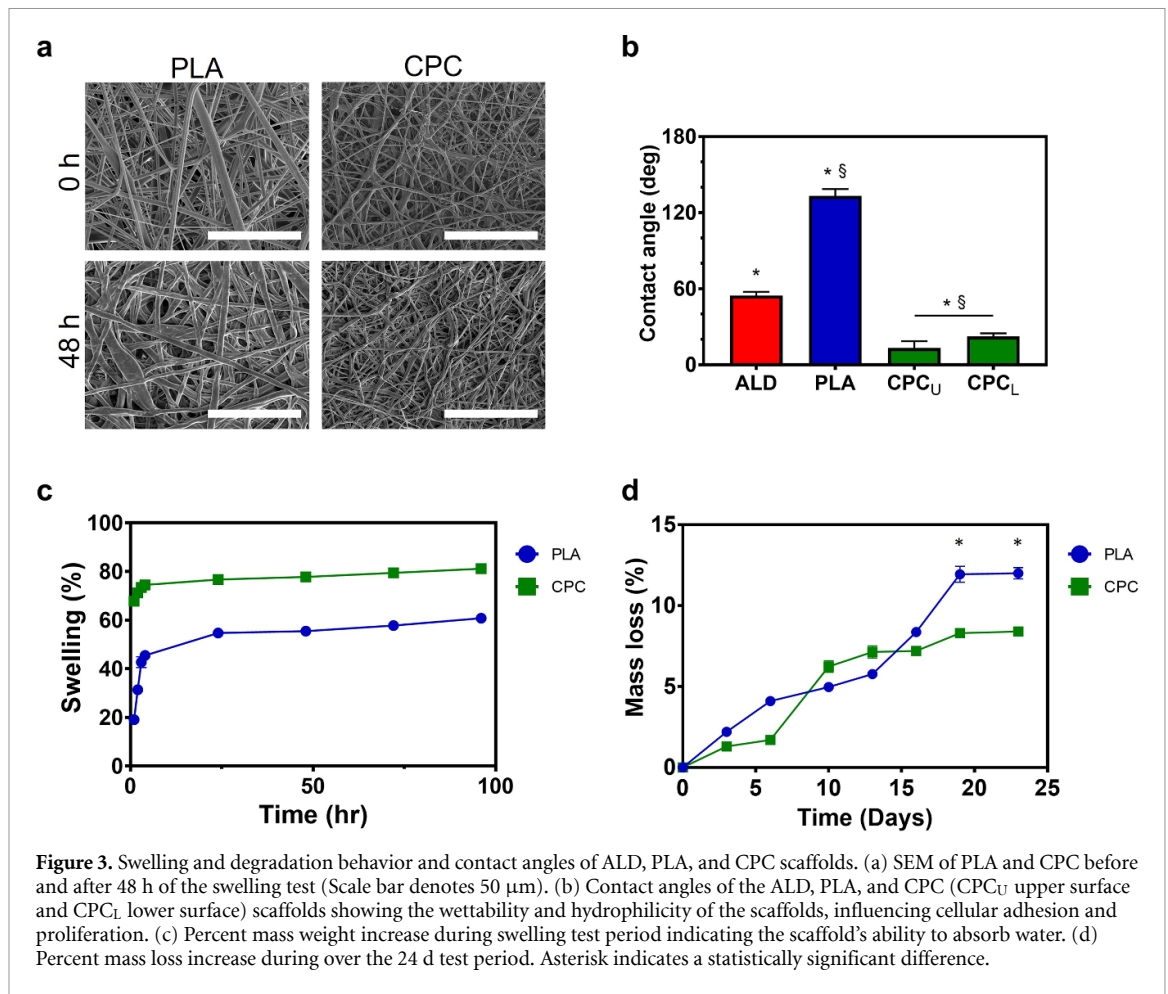
the PLA scaffolds (figure 3(c)). On the other hand, degradation of the scaffold after implantation is a determining factor for clinical success. The evaluation of the weight loss of the scaffolds over time revealed a relatively smaller decrease in the mass of the CPC scaffolds compared to the PLA samples at the end of the observation period (figure 3(d)). Notably, the CPC and PLA scaffolds showed a similar rate of degradation in the first two weeks.

### 3.5. Assessment of cell compatibility

To determine whether the fabricated scaffolds released toxic components that affected cell viability, cultured fibroblasts were exposed to the scaffolds to assess cell viability and migration. As shown in figure 4(a), the number of viable cells was maintained upon exposure to CPC.

Interestingly, exposure to ALD appeared to increase the number of dead cells. This qualitative observation was confirmed by quantitative analysis, which showed that CPC scaffolds, like PLA, had no significant effect on cell viability, whereas exposure to ALD caused a significant decrease in the percentage of viable cells (figure 4(b)). Cell migration is a key determinant of wound closure and healing processes, so fibroblast migration was examined in scratch assays after exposure to the scaffolds. As shown in figure 4(e), the presence of CPC scaffolds increased the rate of wound closure 24 h after monolayer injury. Quantitative analysis shown in figure 4(d) revealed that CPC scaffolds supported  $90.7 \pm 2.1\%$  healing of the fibroblast scratch zone, which was significantly greater compared with the control and PLA groups ( $p < 0.01$ ).





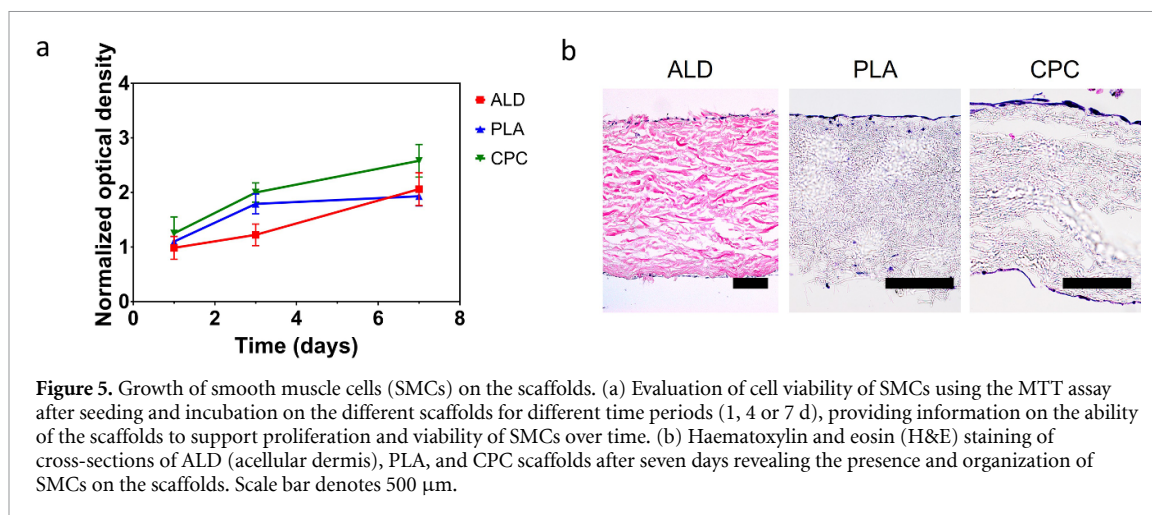


**Figure 5.** Growth of smooth muscle cells (SMCs) on the scaffolds. (a) Evaluation of cell viability of SMCs using the MTT assay after seeding and incubation on the different scaffolds for different time periods (1, 4 or 7 d), providing information on the ability of the scaffolds to support proliferation and viability of SMCs over time. (b) Haematoxylin and eosin (H&E) staining of cross-sections of ALD (acellular dermis), PLA, and CPC scaffolds after seven days revealing the presence and organization of SMCs on the scaffolds. Scale bar denotes 500  $\mu\text{m}$ .

### 3.6. Growth of SMCs on the scaffolds

To assess whether the CPC scaffolds could allow the growth of cells relevant to urethral reconstruction, the ability to support the growth of SMCs was evaluated by cell proliferation assay and histologic analysis (figure 5). SMCs displayed a steady proliferation on CPC scaffolds over the seven-day period (figure 5(a)). CPC scaffolds were able to effectively support SMC growth on both sides of the scaffolds, in contrast to PLA scaffolds where cells appeared to detach from one of the sides (figure 5(b)). This inability to retain cells on the PLA scaffolds was reflected in a decrease in cell proliferation at day 7.

### 3.7. Angiogenesis assay

To assess whether CPC scaffolds can support efficient angiogenesis after transplantation, a chicken embryo-based CAM assay was performed. As shown by the microscope images, the CPC scaffolds formed an adjacent zone of increased vascular density after 24 h (figure 6(a)). Quantitative analysis showed that the CPC scaffolds elicited a significant increase in blood vessel size and number of vessel branches compared with the control (figure 6(b)). The increase in vessel diameter was comparable to that induced by the ALD scaffolds. In contrast, PLA scaffolds had a significantly lower number of vessel branches and no significant effect on vessel diameter.

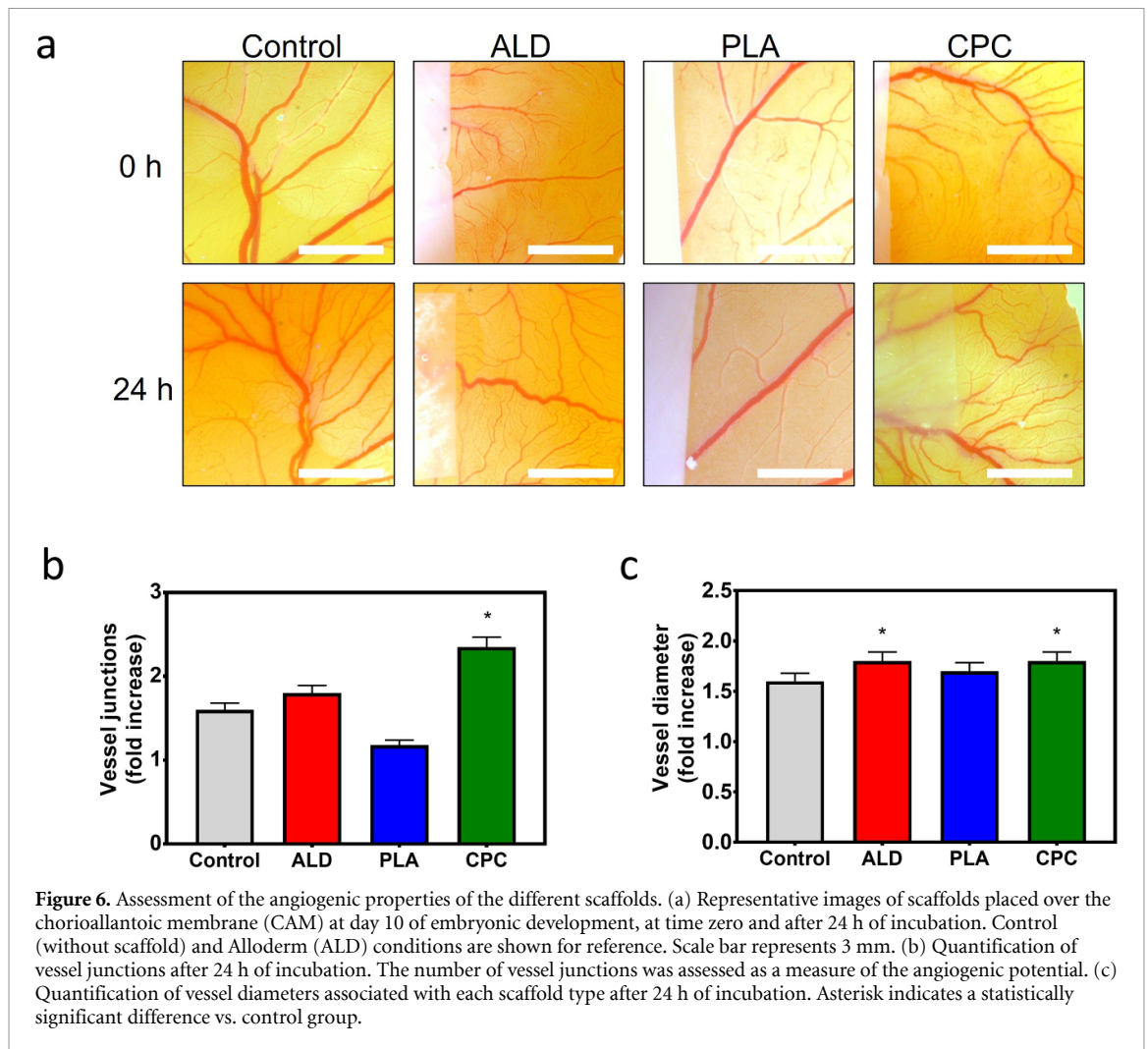
## 4. Discussion

Autologous tissue reconstruction is the current standard for surgical repair of hypospadias and complex long-segment urethral strictures [4, 41, 42]. However, the use of autologous grafts is limited due to donor site morbidity and high complication rates [43–45]. To overcome these limitations, a nanofiber composite scaffold with suitable mechanical and surface properties is proposed to promote efficient cell attachment and growth. The properties of these composite scaffolds (CPC) were compared with Alloderm, a natural

scaffold material composed mainly of type I collagen from human skin [46], and PLA, a synthetic polyester approved for the fabrication of implantable scaffolds. AlloDerm is well established and widely recognized in the field of reconstructive surgery. It was selected as a control material in this study because it is clinically relevant and its value for urethral reconstruction is well documented [47–49]. Morphological assessment of the CPC scaffolds revealed a nano/microfibrous structure, which was supportive of cell growth. It is expected that the favorable growth properties of SMC may also provide good support for other cell types, such as fibroblasts and urethral epithelial cells [50]. The mechanical properties of tissue-engineered scaffolds depend mainly on pore size [51] and fiber structure/interaction [52]. Although the mechanical properties of the implanted scaffolds do not necessarily have to match those of the native tissue, they should be sufficient to maintain an open urethra in the long term. The results of this work show that the addition of chitosan nanofiber layers to the scaffold increased their stiffness, resulting in scaffolds that are easier to manipulate, shape, and handle without undesirable tangles or adhesions. Although the CPC scaffolds failed at high strains ( $\geq 0.5$ ), this value is well above the strains likely to occur after implantation. The higher stiffness of the CPC scaffold would also potentially allow stable implantation of the graft after urethroplasty, with greater tolerance to manipulations associated with transurethral catheterization and voiding pressures.

Suture retention is important for successful graft implantation at critical sites with a high risk of fistula formation, such as the ventral surface of the neourethra and at the junction of the neourethra and meatus [53]. Previous data suggest that scaffold suture retention strength should be  $>0.8$  N for implantation into the urethra [54, 55], and the CPC scaffolds tested here far exceeded this value.

The wettability of a scaffold surface is determined by the balance between hydrophilicity and



hydrophobicity and has a significant impact on cell attachment, proliferation, and viability over time [56]. The presence of chitosan layers significantly increased the wettability of the CPC scaffold, which was reflected by their increased swelling capacity. This is a favorable property which enables efficient cellular infiltration and growth. On the other hand, as expected, the PLA nanofiber scaffolds were highly hydrophobic. SEM images showed that the scaffolds retained their nanofiber structure after immersion in an aqueous medium, suggesting that the increased water-absorption capacity of the CPC scaffolds was due to the increased wettability of the chitosan nanofibers rather than fiber swelling. The rate of degradation of the CPC scaffolds was similar to that reported in the literature, which is approximately 6% over the course of two weeks [57]. However, despite the increased wettability due to the chitosan layers, the CPC scaffolds showed a relatively lower degradation rate than their PLA counterparts. The difference in mass loss between CPC and PLA scaffolds in the later stages can be attributed to the methanol stabilization of the CPC scaffolds. This treatment increases the crystallinity of the polymer, making it less susceptible to degradation in aqueous solutions [38]. The

untreated PLA, which retains an amorphous state, is inherently more susceptible to water penetration and hydrolysis [58]. The degradation of PLA in aqueous solutions is a process that is influenced by several factors, including scaffold shape, molecular weight, crystallinity, and wettability [59]. In our study, the electrospun PLA scaffolds have a high specific surface area and a relatively high molecular weight. Based on this assumption, it can be assumed that PLA is degraded by a hydrolytic process that starts at the surface and within the open-pore nanofiber scaffold [60].

Cell ingrowth into the scaffolds is critical for integration into the surrounding tissue after implantation [61]. Previous studies have shown that scaffold hydrophobicity, physical structure, and biochemical signals can promote cell ingrowth into the scaffold [62]. Electrospun scaffolds with fiber diameters larger than 1  $\mu\text{m}$  and large pore sizes (tens of microns) appear to be well suited to allow cell infiltration, whereas diameters smaller than 1  $\mu\text{m}$  significantly limit infiltration of most cell types [63, 64]. In the current study, SMC cell growth on the CPC scaffold was superior to that of PLA alone. This effect is likely due to the presence of reactive functional

groups in chitosan, which are known to have a positive effect on cell adhesion [65], in contrast to the lack of cell-binding domains in PLA [61].

The degradation components released from the chitosan scaffolds were not cytotoxic and appeared to have a beneficial effect on fibroblast migration. Migration of cells from the wound margin is critical for effective tissue healing [66]. Enhanced migration of fibroblasts into the wound space also leads to rapid deposition of collagen, which may also limit infiltration by proinflammatory cells [67]. CPC scaffolds also showed a beneficial effect on angiogenesis in the CAM assay. This agrees well with previous studies showing that chitosan promotes efficient growth of vascular endothelial cells [68]. Chito-oligomers are known to be released, phosphorylated, and interact with keratan sulphate, chondroitin sulphate, and hyaluronan, all of which influence fibroblast cytokine production and macrophage activation [69]. *In vivo*, fibroblasts can be activated by contact with endothelial cells, either directly or indirectly through the secretion of growth factors, resulting in the production of angiogenic growth factors, including fibroblast growth factor, vascular endothelial growth factor (VEGF), and platelet-derived growth factor [70]. VEGF is an important factor in angiogenesis, promoting tubulogenesis and the formation of 3D networks [71]. It has also been reported that fibroblasts stimulated by chitosan molecules secrete interleukin-8 [72], which is angiogenic and chemotactic to both endothelial and epidermal cells [73].

It is important to recognize certain limitations in our study. First, our research relied predominantly on *in vitro* evaluations, which, while providing valuable insight into the biocompatibility and mechanical properties of the CPC scaffold, do not capture the complex interactions that may occur in a living organism. Secondly, we focused on human bladder SMCs, which, although relevant for evaluating certain aspects, do not include all cell types involved in urethral reconstruction (e.g. urothelial or endothelial cells) [74]. Future research should therefore aim to address these limitations through *in vivo* experiments and the inclusion of a broader range of relevant cell types to ultimately allow a more comprehensive assessment of the suitability of the CPC scaffold for urethral reconstruction.

## 5. Conclusions

It can be concluded that CPC scaffolds have properties that make them a suitable candidate for the surgical repair of hypospadias and long-segment urethral strictures. The nano/microfiber structure of the chitosan layers increases the stiffness of the scaffold, making it easier to handle and process and might provide sufficient mechanical properties to maintain

an open urethra in the long term. The CPC scaffold has high suture retention, which is important for successful graft implantation, and its increased wettability due to the chitosan layers allows for efficient cellular infiltration and growth. CPC scaffolds also have a positive effect on fibroblast migration and angiogenesis, which are critical for effective tissue healing. Overall, the CPC scaffolds represent a promising alternative to autologous tissue reconstruction for the repair of hypospadias and complex long-segment urethral strictures. Future research should include *in vivo* testing in a suitable animal model to determine if these trilayered scaffolds can support host cell ingrowth while functioning as an efficient graft for urethral repair.

## Data availability statement

All data that support the findings of this study are included within the article (and any supplementary files).

## ORCID iDs

Tariq O Abbas  <https://orcid.org/0000-0002-8425-4029>

Huseyin C Yalcin  <https://orcid.org/0000-0003-3825-9934>

Mohamed Hassan  <https://orcid.org/0000-0002-5316-2463>

Cristian P Pennisi  <https://orcid.org/0000-0002-7716-1182>

## References

- [1] Keays M A and Dave S 2017 Current hypospadias management: diagnosis, surgical management, and long-term patient-centred outcomes *Can. Urol. Assoc. J.* **11** S48–53
- [2] Abbas T and McCarthy L 2016 Foreskin and penile problems in childhood *Surg.* **34** 221–5
- [3] Chapple C, Andrich D, Atala A, Barbagli G, Cavalcanti A, Kulkarni S, Mangera A and Nakajima Y 2014 SIU/ICUD consultation on urethral strictures: the management of anterior urethral stricture disease using substitution urethroplasty *Urology* **83** S31–47
- [4] Snodgrass W and Bush N 2016 Primary hypospadias repair techniques: a review of the evidence *Urol. Ann.* **8** 403–8
- [5] Barbagli G, Sansalone S, Djinovic R, Romano G and Lazzeri M 2012 Current controversies in reconstructive surgery of the anterior urethra: a clinical overview *Int. Braz. J. Urol.* **38** 307–16
- [6] Abbas T O, Mahdi E, Hasan A, AlAnsari A and Pennisi C P 2018 Current status of tissue engineering in the management of severe hypospadias *Front. Pediatr.* **5** 283
- [7] Tan Q, Le H, Tang C, Zhang M, Yang W, Hong Y and Wang X 2022 Tailor-made natural and synthetic grafts for precise urethral reconstruction *J. Nanobiotechnol.* **20** 392
- [8] Karam I, Moudouni S, Droupy S, Abd-Alsamad I, Uhl J F and Delmas V 2005 The structure and innervation of the male urethra: histological and immunohistochemical studies with three-dimensional reconstruction *J. Anat.* **206** 395–403
- [9] Kovacs E J 2001 *Wheater's functional histology: a text and colour atlas* vol 125

- [10] Versteegden L R M, de Jonge P K J D, Int'Hout J, van Kuppevelt T H, Oosterwijk E, Feitz W F J, de Vries R B M and Daamen W F 2017 Tissue engineering of the urethra: a systematic review and meta-analysis of preclinical and clinical studies *Eur. Urol.* **72** 594–606
- [11] Orabi H, Bouhout S, Morissette A, Rousseau A, Chabaud S and Bolduc S 2013 Tissue engineering of urinary bladder and urethra: advances from bench to patients *Sci. World J.* **2013** 1–13
- [12] De Kemp V, De Graaf P, Fledderus J O, Bosch J L H R and De Kort L M O 2015 Tissue engineering for human urethral reconstruction: systematic review of recent literature *PLoS One* **10** 1–14
- [13] Bhat A, Bhat M, Kumar V, Kumar R, Mittal R and Saksena G 2016 Comparison of variables affecting the surgical outcomes of tubularized incised plate urethroplasty in adult and pediatric hypospadias *J. Pediatr. Urol.* **12** 108.e1–108.e7
- [14] Bouthour H, Bostame S and Kaabar N 2017 Hypospadias *Pediatr. Surg. Handb. Resid. Med. Students* **2008** 241–57
- [15] Abbas T O, Charles A, Ali M and Pippi Salle J L 2020 Long-term fate of the incised urethral plate in Snodgrass procedure; A real concern does exist *Urol. Case Rep.* **32** 101216
- [16] Yiee J H and Baskin L S 2010 Penile embryology and anatomy *Sci. World J.* **10** 1174–9
- [17] Fu Q and Cao Y-L 2012 Tissue engineering and stem cell application of urethroplasty: from bench to bedside *Urology* **79** 246–53
- [18] Palmer B W and Kropp B P 2013 Update on tissue engineering in pediatric urology *Curr. Urol. Rep.* **14** 327–32
- [19] Sartoneva R, Haaparanta A-M, Lahdes-Vasama T, Mannerström B, Kellomäki M, Salomäki M, Sándor G, Seppänen R, Miettinen S and Haimi S 2012 Characterizing and optimizing poly-L-lactide-co- $\epsilon$ -caprolactone membranes for urothelial tissue engineering *J. R. Soc. Interface* **9** 3444–54
- [20] Sartoneva R, Nordback P H, Haimi S, Grijpma D W, Lehto K, Rooney N, Seppänen-Kaijansinkko R, Miettinen S and Lahdes-Vasama T 2018 Comparison of poly(L-lactide-co- $\epsilon$ -caprolactone) and poly(trimethylene carbonate) membranes for urethral regeneration: an *in vitro* and *in vivo* study *Tissue Eng. A* **24** 117–27
- [21] Abbas T O, Yalcin H C and Pennisi C P 2019 From acellular matrices to smart polymers: degradable scaffolds that are transforming the shape of urethral tissue engineering *Int. J. Mol. Sci.* **20** 1763
- [22] Cheng Y, Deng S, Chen P and Ruan R 2009 Polylactic acid (PLA) synthesis and modifications: a review *Front. Chem. China* **4** 259–64
- [23] Coutu D L, Yousefi A M and Galipeau J 2009 Three-dimensional porous scaffolds at the crossroads of tissue engineering and cell-based gene therapy *J. Cell Biochem.* **108** 537–46
- [24] Papenburg B J, Liu J, Higuera G A, Barradas A M C, de Boer J, van Blitterswijk C A, Wessling M and Stamatialis D 2009 Development and analysis of multi-layer scaffolds for tissue engineering *Biomaterials* **30** 6228–39
- [25] Liu X and Ma P X 2004 Polymeric scaffolds for bone tissue engineering *Ann. Biomed. Eng.* **32** 477–86
- [26] Hu J, Ai B, Zhu S, Wang Z, Xia H and Jia W 2022 Electrospun PLGA and PLGA/gelatin scaffolds for tubularized urethral replacement: studies *in vitro* and *in vivo* *J. Biomater. Appl.* **36** 956–64
- [27] Simsek A, Bullock A J, Roman S, Chapple C R and MacNeil S 2018 Developing improved tissue-engineered buccal mucosa grafts for urethral reconstruction *Can. Urol. Assoc. J.* **12** E234–42
- [28] Casarin M, Todesco M, Sandrin D, Romanato F, Bagno A, Morlacco A and Dal Moro F 2022 A novel hybrid membrane for urinary conduit substitutes based on small intestinal submucosa coupled with two synthetic polymers *J. Funct. Biomater.* **13** 222
- [29] Rinaudo M 2006 Chitin and chitosan: properties and applications *Prog. Polym. Sci.* **31** 603–32
- [30] Aranaz I, Mengibar M, Harris R, Panos I, Miralles B, Acosta N, Galed G and Heras A 2012 Functional characterization of chitin and chitosan *Curr. Chem. Biol.* **3** 203–30
- [31] Decher G 1997 Fuzzy nanoassemblies: toward layered polymeric multicomposites *Science* **277** 1232–7
- [32] Dash M, Chiellini F, Ottenbrite R M and Chiellini E 2011 Chitosan—A versatile semi-synthetic polymer in biomedical applications *Prog. Polym. Sci.* **36** 981–1014
- [33] Pangburn S H, Trescony P V and Heller J 1982 Lysozyme degradation of partially deacetylated chitin, its films and hydrogels *Biomaterials* **3** 105–8
- [34] Raafat D and Sahl H G 2009 Chitosan and its antimicrobial potential—A critical literature survey *Microb. Biotechnol.* **2** 186–201
- [35] Bhattarai N, Edmondson D, Veishe O, Matsen F A and Zhang M 2005 Electrospun chitosan-based nanofibers and their cellular compatibility *Biomaterials* **26** 6176–84
- [36] Horst M, Madduri S, Milleret V, Sulser T, Gobet R and Eberli D 2013 A bilayered hybrid microfibrillar PLGA-Acellular matrix scaffold for hollow organ tissue engineering *Biomaterials* **34** 1537–45
- [37] Abbas T O, Ali T A and Uddin S 2020 Urine as a main effector in urological tissue engineering—a double-edged sword *Cells* **9** 538
- [38] Judawisastro H, Hadyiswanto I O C, Sitohang R D R and Winiati W 2015 Improvements of tensile properties and durability of chitosan fiber using methanol drying treatment *Macromol. Symp.* **353** 147–53
- [39] El-Gomati M M, Walker C G H, Bonet C, Tear S P and Matthew J A D 2008 Secondary, backscattered and low energy loss electrons in the SEM: quantification for nano analysis *Microsc. Microanal.* **14** 908–9
- [40] Hotaling N A, Bharti K, Kriel H and Simon Carl G J 2015 DiameterJ: a validated open source nanofiber diameter measurement tool *Biomaterials* **61** 327–38
- [41] Mathur R K, Nagar M, Mathur R, Khan F, Deshmukh C and Guru N 2014 Single-stage preputial skin flap urethroplasty for long-segment urethral strictures: evaluation and determinants of success *BJU Int.* **113** 120–6
- [42] Kozinn S I, Harty N J, Zinman L and Buckley J C 2013 Management of complex anterior urethral strictures with multistage buccal mucosa graft reconstruction *Urology* **82** 718–23
- [43] Mori R L and Angermeier K W 2015 Staged urethroplasty in the management of complex anterior urethral stricture disease *Transl. Androl. Urol.* **4** 29–34
- [44] Spinoit A F et al 2021 Fertility and sexuality issues in congenital lifelong urology patients: male aspects *World J. Urol.* **39** 1013–9
- [45] Fabbri G, Loukota R A A and Eardley I 2005 Buccal mucosal grafts for urethroplasty: surgical technique and morbidity *Br. J. Oral Maxillofac. Surg.* **43** 320–3
- [46] Gouk S S, Lim T M, Teoh S H and Sun W Q 2008 Alterations of human acellular tissue matrix by gamma irradiation: histology, biomechanical property, stability, *in vitro* cell repopulation, and remodeling *J. Biomed. Mater. Res. B* **84** 205–17
- [47] Carpenter C P, Daniali L N, Shah N P, Granick M and Jordan M L 2012 Distal urethral reconstruction with AlloDerm: a case report and review of the literature *Can. J. Urol.* **19** 6207–10
- [48] Morgante D, Radford A, Abbas S K, Ingham E, Subramaniam R and Southgate J 2021 Augmentation of the insufficient tissue bed for surgical repair of hypospadias using acellular matrix grafts: a proof of concept study *J. Tissue Eng.* **12** 204173142199884
- [49] Wu S, Ye C, Yang H, Chen B, Nie H and Li S 2022 Application of allogeneic human acellular dermal matrix reduces the incidence of fistula in hypospadias repair *Front. Pediatr.* **10** 774973

- [50] Lin C Q and Bissell M J 1993 Multi-faceted regulation of cell differentiation by extracellular matrix *FASEB J.* **7** 737–43
- [51] Darbasizadeh B, Motasadizadeh H, Foroughi-Nia B and Farhadnejad H 2018 Tripolyphosphate-crosslinked chitosan/poly (ethylene oxide) electrospun nanofibrous mats as a floating gastro-retentive delivery system for ranitidine hydrochloride *J. Pharm. Biomed. Anal.* **153** 63–75
- [52] Qasim S B, Najeeb S, Delaine-Smith R M, Rawlinson A and Ur Rehman I 2017 Potential of electrospun chitosan fibers as a surface layer in functionally graded GTR membrane for periodontal regeneration *Dent. Mater.* **33** 71–83
- [53] Romagnoli G, De Luca M, Faranda F, Bandelloni R, Franzini A T, Cataliotti F and Cancedda R 1990 Treatment of posterior hypospadias by the autologous graft of cultured urethral epithelium *New Engl. J. Med.* **323** 527–30
- [54] Wang S, Zhang Y, Wang H, Yin G and Dong Z 2009 Fabrication and properties of the electrospun polylactide/silk fibroin-gelatin composite tubular scaffold *Biomacromolecules* **10** 2240–4
- [55] Fan S, Zhang Y, Shao H and Hu X 2013 Electrospun regenerated silk fibroin mats with enhanced mechanical properties *Int. J. Biol. Macromol.* **56** 83–88
- [56] Zhang D *et al* 2015 Electrospun SF/PLCL nanofibrous membrane: a potential scaffold for retinal progenitor cell proliferation and differentiation *Sci. Rep.* **5** 14326
- [57] Lončarević A, Ivanković M and Rogina A 2017 Lysozyme-induced degradation of chitosan: the characterisation of degraded chitosan scaffolds *J. Tissue Repair. Regen.* **1** 12–22
- [58] Sato S, Gondo D, Wada T, Kanehashi S and Nagai K 2013 Effects of various liquid organic solvents on solvent-induced crystallization of amorphous poly(lactic acid) film *J. Appl. Polym. Sci.* **129** 1607–17
- [59] Middleton J C and Tipton A J 2000 Synthetic biodegradable polymers as orthopedic devices *Biomaterials* **21** 2335–46
- [60] Magiera A, Markowski J, Pilch J and Blazewicz S 2018 Degradation behavior of electrospun PLA and PLA/CNT nanofibres in aqueous environment *J. Nanomater.* **2018** 1–15
- [61] Sachlos E and Czernuszka J 2003 Making tissue engineering scaffolds work. Review: the application of solid freeform fabrication technology to the production of tissue engineering scaffolds *Eur. Cells Mater.* **5** 29–40
- [62] Zhong S, Zhang Y and Lim C T 2012 Fabrication of large pores in electrospun nanofibrous scaffolds for cellular infiltration: a review *Tissue Eng. B* **18** 77–87
- [63] Lowery J L, Datta N and Rutledge G C 2010 Effect of fiber diameter, pore size and seeding method on growth of human dermal fibroblasts in electrospun poly( $\epsilon$ -caprolactone) fibrous mats *Biomaterials* **31** 491–504
- [64] Badami A S, Kreke M R, Thompson M S, Riffle J S and Goldstein A S 2006 Effect of fiber diameter on spreading, proliferation, and differentiation of osteoblastic cells on electrospun poly(lactic acid) substrates *Biomaterials* **27** 596–606
- [65] Rodríguez-Vázquez M, Vega-Ruiz B, Ramos-Zúñiga R, Saldaña-Koppel D A and Quiñones-Olvera L F 2015 Chitosan and its potential use as a scaffold for tissue engineering in regenerative medicine *Biomed. Res. Int.* **2015** 821279
- [66] Velnar T, Bailey T and Smrkolj V 2009 The wound healing process: an overview of the cellular and molecular mechanisms *J. Int. Med. Res.* **37** 1528–42
- [67] McDougall S, Dallon J, Sherratt J and Maini P 2006 Fibroblast migration and collagen deposition during dermal wound healing: mathematical modelling and clinical implications *Phil. Trans. R. Soc. A* **364** 1385–405
- [68] Zhang L, Ao Q, Wang A, Lu G, Kong L, Gong Y, Zhao N and Zhang X 2006 A sandwich tubular scaffold derived from chitosan for blood vessel tissue engineering *J. Biomed. Mater. Res. A* **77** 277–84
- [69] Muzzarelli R A, Mattioli-Belmonte M, Pugnali A and Biagini G 1999 Biochemistry, histology and clinical uses of chitins and chitosans in wound healing *EXS* **87** 251–64
- [70] Velázquez O C, Snyder R, Liu Z J, Fairman R M and Herlyn M 2002 Fibroblast-dependent differentiation of human microvascular endothelial cells into capillary-like 3-dimensional networks *FASEB J.* **16** 1316–8
- [71] Kellouche S, Mourah S, Bonnefoy A, Schoëvaert D, Podgorniak M P, Calvo F, Hoylaerts M F, Legrand C and Dosquet C 2007 Platelets, thrombospondin-1 and human dermal fibroblasts cooperate for stimulation of endothelial cell tubulogenesis through VEGF and PAI-1 regulation *Exp. Cell Res.* **313** 486–99
- [72] Mori T, Okumura M, Matsuura M, Ueno K, Tokura S, Okamoto Y, Minami S and Fujinaga T 1997 Effects of chitin and its derivatives on the proliferation and cytokine production of fibroblasts *in vitro Biomaterials* **18** 947–51
- [73] Koch A E, Polverini P J, Kunkel S L, Harlow L A, DiPietro L A, Elner V M, Elner S G and Strieter R M 1992 Interleukin-8 as a Macrophage-Derived Mediator of Angiogenesis *Science* **258** 1798–801
- [74] Xuan Z, Zachar V and Pennisi C P 2022 Sources, selection, and microenvironmental preconditioning of cells for urethral tissue engineering *Int. J. Mol. Sci.* **23** 14074